Published in IET Microwaves, Antennas & Propagation
Received on 26th April 2010
Revised on 26th August 2010
doi: 10.1049/iet-map.2010.0166

ISSN 1751-8725

Blind direction-of-arrival estimation algorithm for conformal array antenna with respect to polarisation diversity

Z.-s. Qi Y. Guo B.-h. Wang

Institute of Telecommunication Engineering, Air Force Engineering University, Xi'an 710077, People's Republic of China
E-mail: qizisen@163.com

Abstract: Owing to the curvature of the conformal carrier, the polarisation diversity of element patterns is one of the most distinct characteristics of conformal array manifolds. Consequently, direction-of-arrival (DOA) estimation with conformal array antennas always couples with the estimation of the polarisation. Based on the fourth-order cumulants of the array outputs and an elaborately designed array structure, an estimation of signal parameters via rotational invariance techniques-based blind DOA estimation algorithm with respect to polarisation diversity is proposed for conformal array antennas, in which the displacement vectors required by ESPRIT are acquired by utilising 'virtual array elements' derived from actual array elements by 'virtual cross-correlation computation'. Owing to the fact that these distance vectors used in algorithm implementation are not affected by element patterns and source polarisation, the 2D DOA estimates are decoupled from polarisation and obtained with no need for exact knowledge of array element polarised patterns. The proposed method achieves high-resolution 2D DOA estimation and is applicable to cylindrical, conical and spherical conformal carriers. The array set-up examples of conical, cylindrical and spherical carriers are presented for demonstration and the Monte-Carlo simulation results of DOA estimation with cylindrical conformal array are also provided to illustrate the effectiveness of the proposed algorithm.

1 Introduction

Conformal array antennas [1] will find promising applications in a variety of fields ranging from space-borne, airborne, ship-borne, missile-borne radar, space vehicles and wireless communications to sonar. Their benefits include reduction of aerodynamic drag, wide-angle coverage, reduced space, potential increase in available aperture, reduction of radar cross-section, elimination of radome-induced bore-sight error and so on. There is an increasing demand for implementing fast and precise direction-of-arrival (DOA) estimation with conformal array antennas. Owing to the varying normal of the carrier, the polarisation diversity of array element patterns is one of the most distinct characteristics of conformal array manifolds [2]. This leads to an intractable problem for DOA estimation with conformal array antennas: the estimation of the source polarisation is always accompanied by the DOA estimation because the source polarisation is necessary for precise modelling of the conformal array. This means that the polarisation parameters and DOA of incident sources are required to be estimated jointly. Considering this troublesome coupling between DOA and polarisation, the most conventional algorithms [3–7] and their performance analysis approaches [8–12] for classical array structure cannot be directly applied to conformal arrays.

Among the high-resolution DOA estimation methods for conformal array reported recently [13–19], the conventional DOA estimation method is extended to joint polarisation and DOA estimation in [13], but the different local Cartesian coordinates of different array elements are not considered at all. Performance analysis of classical algorithms for conformal arrays is discussed in [14], but the polarisation diversity of conformal array manifolds is ignored. With the aim to transform conformal manifold into classical uniform linear array manifold, array transform techniques are used in [15, 16]. Based on the manifold transformation, the adverse effect of element pattern on DOA estimation performance is somewhat mitigated, but the algorithm is limited by the field-of-view (FOV) and is sensitive to the error in manifold transformation. A generic modelling method for conformal array manifold is proposed in [2, 17], in which a spatial rotation transformation is exploited to describe the different local Cartesian coordinates for the element-polarised pattern. Performance analysis of multiple signal classification [3] for conformal array antennas is presented in [18], which investigates the effect of element pattern on the performance of DOA estimation, but prior knowledge of the source polarisation is assumed.

In the simplified array data model assumed in almost all the papers mentioned above, the polarisation diversity is not considered at all, which is unrealistic in practical applications. Recently, a blind DOA estimation method with respect to polarisation diversity was proposed for conical conformal array antenna [19], in which three pairs of special subarrays are exploited and 2D DOA estimation are achieved without knowing the polarisation parameters.

However, this algorithm was developed for conical arrays only, and cannot be extended to the case of other conformal array geometries. Based on the fourth-order (FO) cumulants of array measurements and an elaborately designed array structure, a blind DOA estimation algorithm for conformal array antenna is proposed in this paper. The new algorithm is applicable to cylindrical, conical and spherical carriers and achieves high-resolution DOA estimation without exact knowledge of the signal polarisation. The array design examples of conical, cylindrical and spherical carriers are presented for demonstration. Monte-Carlo simulation results of DOA estimation with cylindrical conformal array are also provided to illustrate the effectiveness of the proposed algorithm.

The outline of this paper is as follows. Section 2 presents the conformal array data model and a discussion on the distinct characteristics of DOA estimation with conformal arrays. A simple review of the application of FO cumulants to aperture extension is addressed in Section 3, in which the mechanism of 'virtual cross-correlation computation' (VC^3) [20] is emphasised for the theoretical preparation of the proposed method. The array element deployments on conical, cylindrical and spherical carriers are described in Section 4. A blind DOA estimation algorithm with respect to polarisation diversity is proposed in Section 5. To illustrate the effectiveness of the proposed algorithm, computer simulations are presented in Section 6. Finally, Section 7 concludes this paper.

2 Conformal array data model

Consider an array of m array elements that conforms to the arbitrary 3D geometry in Fig. 1 and is impinged by a plane wave from far-field sources with elevation θ and azimuth ϕ. For the scenario that the normals of element patterns are identical, the corresponding array steering vector can be expressed as follows

$$\boldsymbol{a}_{\text{classical}}(\theta, \phi) = [\mathrm{e}^{-\mathrm{j}2\pi(\boldsymbol{P}_1\boldsymbol{u}/\lambda)}, \mathrm{e}^{-\mathrm{j}2\pi(\boldsymbol{P}_2\boldsymbol{u}/\lambda)}, \ldots, \mathrm{e}^{-\mathrm{j}2\pi(\boldsymbol{P}_m\boldsymbol{u}/\lambda)}]^{\mathrm{T}} \tag{1}$$

$$\boldsymbol{u} = \sin(\theta)\cos(\phi)\boldsymbol{X} + \sin(\theta)\sin(\phi)\boldsymbol{Y} + \cos(\theta)\boldsymbol{Z} \tag{2}$$

where $\boldsymbol{u}$ denotes the propagation vector, λ is the wavelength and $\boldsymbol{P}_i$ is the position vector of the ith element.

However, conformal arrays manifest themselves with different element patterns and orientations because of the varying curvature of carriers. Hence, the effect of element patterns must be taken into account in the establishment of the array data model for the conformal array antennas and this leads to the polarisation diversity of the conformal array manifold. As the element pattern is always defined in its local coordinate system, a spatial rotation transformation is necessary to find the element pattern in the global coordinate system. The generic modelling method for an arbitrary conformal array is presented by exploiting the spatial rotation transform of element pattern in [2, 17]. On this basis, the steering vector of conformal array illuminated by far-field narrowband signals takes the form

$$\boldsymbol{a}_{\text{conformal}}(\theta, \phi) = \left[r_1\mathrm{e}^{-\mathrm{j}2\pi\frac{\boldsymbol{P}_1\boldsymbol{u}}{\lambda}}, r_2\mathrm{e}^{-\mathrm{j}2\pi\frac{\boldsymbol{P}_2\boldsymbol{u}}{\lambda}}, \ldots, r_m\mathrm{e}^{-\mathrm{j}2\pi\frac{\boldsymbol{P}_m\boldsymbol{u}}{\lambda}}\right]^{\mathrm{T}} \tag{3}$$

$$\begin{aligned} r_i &= (g_{i\theta}^2+g_{i\phi}^2)^{1/2}(k_\theta^2+k_\phi^2)^{1/2}\cos(\theta_{igk}) \\ &= |\boldsymbol{g}_i||\boldsymbol{p}_l|\cos(\theta_{igk}) = \boldsymbol{g}_i\boldsymbol{p}_l = g_{i\theta}k_\theta + g_{i\phi}k_\phi \end{aligned} \tag{4}$$

where $\boldsymbol{u}_\theta$ and $\boldsymbol{u}_\phi$ are unit vectors [2], k_θ, k_ϕ are the polarisation parameters of signal, $\boldsymbol{g}_i$ denotes the pattern of the ith element, $\boldsymbol{p}_i$ is the direction of electric field and r_i is the response of unit signal by the ith element in a global coordinate system as in Fig. 2. θ_{igk} denotes the angle between vector $\boldsymbol{g}_i$ and vector $\boldsymbol{p}_i$. If there are n sources and m array elements, the snapshot model can be expressed as follows

$$\boldsymbol{X} = \boldsymbol{A}\boldsymbol{S} + \boldsymbol{N} = (\boldsymbol{A}_\theta\boldsymbol{K}_\theta + \boldsymbol{A}_\phi\boldsymbol{K}_\phi)\boldsymbol{S} + \boldsymbol{N} \tag{5}$$

$$\boldsymbol{S} = [s_1, s_2, \ldots, s_n]^{\mathrm{T}} \tag{6}$$

$$\boldsymbol{N} = [n_1, n_2, \ldots, n_n]^{\mathrm{T}} \tag{7}$$

$$\boldsymbol{A}_\theta = [\boldsymbol{a}_\theta(\theta_1, \phi_1), \boldsymbol{a}_\theta(\theta_2, \phi_2), \ldots, \boldsymbol{a}_\theta(\theta_n, \phi_n)] \tag{8}$$

$$\boldsymbol{A}_\phi = [\boldsymbol{a}_\phi(\theta_1, \phi_1), \boldsymbol{a}_\phi(\theta_2, \phi_2), \ldots, \boldsymbol{a}_\phi(\theta_n, \phi_n)] \tag{9}$$

$$\boldsymbol{K}_\theta = \mathrm{diag}(k_{1\theta}, k_{2\theta}, \ldots, k_{n\theta}) \tag{10}$$

$$\boldsymbol{K}_\phi = \mathrm{diag}(k_{1\phi}, k_{2\phi}, \ldots, k_{n\phi}) \tag{11}$$

$$\begin{aligned} &\boldsymbol{a}_\theta(\theta_i, \phi_i) \\ &= [g_{1\theta}\mathrm{e}^{-\mathrm{j}2\pi(\boldsymbol{P}_1\boldsymbol{u}_i/\lambda)}, g_{2\theta}\mathrm{e}^{-\mathrm{j}2\pi(\boldsymbol{P}_2\boldsymbol{u}_i/\lambda)}, \ldots, g_{m\theta}\mathrm{e}^{-\mathrm{j}2\pi(\boldsymbol{P}_m\boldsymbol{u}_i/\lambda)}]^{\mathrm{T}} \end{aligned} \tag{12}$$

$$\begin{aligned} &\boldsymbol{a}_\phi(\theta_i, \phi_i) \\ &= [g_{1\phi}\mathrm{e}^{-\mathrm{j}2\pi(\boldsymbol{P}_1\boldsymbol{u}_i/\lambda)}, g_{2\phi}\mathrm{e}^{-\mathrm{j}2\pi(\boldsymbol{P}_2\boldsymbol{u}_i/\lambda)}, \ldots, g_{m\phi}\mathrm{e}^{-\mathrm{j}2\pi(\boldsymbol{P}_m\boldsymbol{u}_i/\lambda)}]^{\mathrm{T}} \end{aligned} \tag{13}$$

where $\boldsymbol{A}$ is the full-rank steering matrix, $\boldsymbol{s}$ denotes the source waveforms and $\boldsymbol{N}$ is the noise contribution. $\boldsymbol{K} = \mathrm{diag}(k_1, k_2, \ldots, k_n)$ is a diagonal matrix with the diagonal entries as

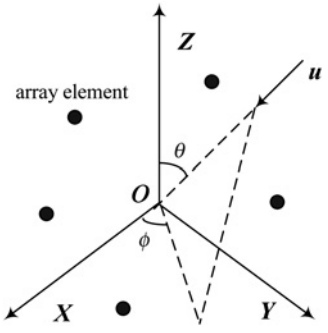

Fig. 1 *Arbitrary 3D array antenna*

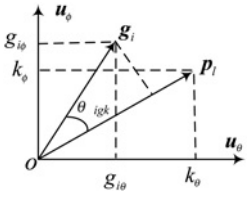

Fig. 2 *Response of the ith element in the global coordinate system*

doi: 10.1049/iet-map.2010.0166

$k_1, k_2, \ldots, k_n$. θ_i, ϕ_i are the 2D DOA of the ith signal illuminating the array. $k_{i\theta}$, $k_{i\phi}$ are the polarisation parameters of the ith signal. They are the components of the electromagnetic wave along the unit vectors $\boldsymbol{u}_\theta$ and $\boldsymbol{u}_\phi$.

It can be observed from (3)–(13) that both DOA and polarisation parameters are embedded in parameterisation of the outputs of conformal array antennas. Therefore the primary difficulties and characteristics of DOA estimation with conformal array can be concluded as follows:

1. Owing to the different element orientations, polarisation diversity occurs in the conformal array manifold.
2. Both DOA and polarisation parameters are contained in formulations of the snapshots of the conformal array.
3. DOA and polarisation should be estimated jointly or decoupled with each other.

In light of the above characteristics of conformal arrays, the main aim of this paper is to propose a polarisation-decoupled DOA estimation algorithm for conformal array antennas. When the snapshots are assumed to be composed of non-Gaussian signals and additive Gaussian noise component, the estimation of signal parameters via rotational invariance techniques (ESPRIT) algorithm [6] and FO cumulants calculation of array measurements are explored to decouple DOA estimation from the polarisation estimation.

3 Application of FO cumulants to aperture extension

In order to find the source DOA using the ESPRIT algorithm, the paired subarrays with displacement vector and identical set-up are necessary. When there are n parameters to be estimated, n pairs subarrays with different displacement vectors are required by the ESPRIT algorithm. The information necessary to estimate parameters is all embedded in the phases in the displacement vectors. If there are enough paired subarrays in the conformal array and the corresponding displacement vectors are independent of element patterns, the DOA of sources can be found blindly with respect to polarisation diversity. However, the special array configuration required by the ESPRIT algorithm is not always available in general conformal arrays because of their arbitrary geometries and different element patterns.

When independent far-field sources emit non-Gaussian plane signals and the noise contribution is additive Gaussian random processes (spatial-white or coloured), FO cumulants calculation of conformal array measurements can be exploited to implement the high-resolution DOA estimation. An interpretation for the use of FO cumulants in narrowband array-processing problems is presented in [20], where it is shown how FO cumulants of observations increase the effective aperture of array. With the help of virtual array elements derived from VC^3 presented in [20], it is possible to implant the ESPRIT algorithm to conformal array antennas. The cross-correlation between actual and virtual array element outputs can be computed by FO cumulants of actual array element outputs, because the FO cumulants can be interpreted as a vector addition. In other words, the array element number increases because of the usage of higher-order statistics (HOS), and the 'extended steering vector' consists of actual and virtual array elements can be established accordingly. The details of the 'extended steering vector' can be formulated as follows.

Given an array of m array elements, and $\boldsymbol{u}$ being the propagation vector, the steering vector takes the form

$$\boldsymbol{a}(\theta, \phi) = [r_1 \exp(-\mathrm{j}k_0\boldsymbol{p}_1 \cdot \boldsymbol{u}), \ldots, r_m \exp(-\mathrm{j}k_0\boldsymbol{p}_m \cdot \boldsymbol{u})] \quad (14)$$

where $k_0 = 2\pi/\lambda$. The 'extended steering vector' is the Kronecker product between the original steering vector and its conjugated operation

$$\begin{aligned}
\boldsymbol{b}(\theta, \phi) &= \boldsymbol{a}(\theta, \phi) \otimes \boldsymbol{a}^*(\theta, \phi) \\
&= [r_1 \exp(-\mathrm{j}k_0\boldsymbol{p}_1 \cdot \boldsymbol{u}), \ldots, r_m \exp(-\mathrm{j}k_0\boldsymbol{p}_m \cdot \boldsymbol{u})] \\
&\quad \otimes [r_1 \exp(\mathrm{j}k_0\boldsymbol{p}_1 \cdot \boldsymbol{u}), \ldots, r_m \exp(\mathrm{j}k_0\boldsymbol{p}_m \cdot \boldsymbol{u})] \\
&= [r_1^2, r_1 r_2 \exp\{-\mathrm{j}k_0(\boldsymbol{p}_1 - \boldsymbol{p}_2) \cdot \boldsymbol{u}\}, \ldots, \\
&\quad r_1 r_m \exp\{-\mathrm{j}k_0(\boldsymbol{p}_1 - \boldsymbol{p}_m) \cdot \boldsymbol{u}\} \\
&\quad r_2 r_1 \exp\{-\mathrm{j}k_0(\boldsymbol{p}_2 - \boldsymbol{p}_1) \cdot \boldsymbol{u}\}, g_2^2, \ldots, \\
&\quad r_2 r_m \exp\{-\mathrm{j}k_0(\boldsymbol{p}_2 - \boldsymbol{p}_m) \cdot \boldsymbol{u}\} \\
&\quad \vdots \\
&\quad r_m r_1 \exp\{-\mathrm{j}k_0(\boldsymbol{p}_m - \boldsymbol{p}_1) \cdot \boldsymbol{u}\}, \ldots, \\
&\quad r_m r_{m-1} \exp\{-\mathrm{j}k_0(\boldsymbol{p}_m - \boldsymbol{p}_{m-1}) \cdot \boldsymbol{u}, r_m^2\}]
\end{aligned} \quad (15)$$

where $\otimes$ denotes the Kronecker product, and $(\cdot)^*$ denotes the conjugated operation. When the array element outputs consist of narrowband far-field independent non-Gaussian signals and additive Gaussian noise, FO cumulants can suppress Gaussian components and the covariance matrix of extended array outputs can be expressed as follows [21]

$$\begin{aligned}
&\boldsymbol{R}_{\mathrm{cum4}}((k_1 - 1)2m + k_3, (k_2 - 1)2m + k_4) \\
&\quad = \mathrm{cum}\{\boldsymbol{x}_{k_1}(t), \boldsymbol{x}_{k_2}(t), \boldsymbol{x}_{k_3}^{\mathrm{H}}(t), \boldsymbol{x}_{k_4}^{\mathrm{H}}(t)\} \\
&\quad = \boldsymbol{B}(\theta, \phi)\boldsymbol{C}_4\boldsymbol{B}^{\mathrm{H}}(\theta, \phi)
\end{aligned} \quad (16)$$

$$\begin{aligned}
\boldsymbol{B}(\theta, \phi) &= [\boldsymbol{A}(\theta, \phi) \otimes \boldsymbol{A}^*(\theta, \phi)] \\
&= [a(\theta_1, \phi_1) \otimes a^*(\theta_1, \phi_1), a(\theta_1, \phi_1) \\
&\quad \otimes a^*(\theta_2, \phi_2), \ldots, a(\theta_1, \phi_1) \otimes a^*(\theta_n, \phi_n) \\
&\quad a(\theta_2, \phi_2) \otimes a^*(\theta_1, \phi_1), a(\theta_2, \phi_2) \\
&\quad \otimes a^*(\theta_2, \phi_2), \ldots, a(\theta_2, \phi_2) \otimes a^*(\theta_n, \phi_n) \\
&\quad \vdots \\
&\quad a(\theta_n, \phi_n) \otimes a^*(\theta_1, \phi_1), a(\theta_n, \phi_n) \\
&\quad \otimes a^*(\theta_2, \phi_2), \ldots, a(\theta_n, \phi_n) \otimes a^*(\theta_n, \phi_n)]
\end{aligned} \quad (17)$$

$$\begin{aligned}
&\boldsymbol{C}_4((l_1 - 1)n + l_3, (l_2 - 1)n + l_4) \\
&\quad = \mathrm{cum}\{\boldsymbol{s}_{l_1}(t), \boldsymbol{s}_{l_2}(t), \boldsymbol{s}_{l_3}^{\mathrm{H}}(t), \boldsymbol{s}_{l_4}^{\mathrm{H}}(t)\}
\end{aligned} \quad (18)$$

where $\boldsymbol{R}_{\mathrm{cum4}}(i, j)$ denotes the element of matrix $\boldsymbol{R}_{\mathrm{cum4}}$ in the ith row and the jth column. $\boldsymbol{C}_4(i, j)$ is the element of matrix $\boldsymbol{C}_4$ in the ith row and the jth column. $\boldsymbol{x}_{k_i}(t)$ denotes the outputs of the k_ith array element, and $k_i \in (1,2, \ldots, 2m)$. $\boldsymbol{s}_{l_i}(t)$ is the signal emitted from the l_ith source, and $l_i \in (1,2, \ldots, n)$. There are only n non-zero elements in matrix $\boldsymbol{C}_4$, since signals are zero-mean non-Gaussian independent random processes and the noise is a zero-mean Gaussian (spatial-white or coloured) random process. The non-zero elements multiplied by $a(\theta_i,\varphi_i) \otimes a^*(\theta_i,\varphi_i)$ (shown in (14)) are obtained in the case of $l_1 = l_2 = l_3 = l_4$.

Observe from (15) that, the difference between elements $r_i r_j \exp\{-jk_0(\boldsymbol{p}_i - \boldsymbol{p}_j)\cdot\boldsymbol{u}\}$ and $r_j r_i\{\exp -jk_0(\boldsymbol{p}_j - \boldsymbol{p}_i)\cdot\boldsymbol{u}\}(i \neq j)$ in vector $\boldsymbol{b}(\theta, \varphi)$ is the phase difference, which is not affected by element patterns and source polarisation. On this basis, the paired subarrays required by the ESPRIT algorithm can be constructed through choosing virtual array elements from the 'extended steering vector', and the corresponding displacement vectors are not affected by element patterns (as shown in the following section in detail). So based on virtual array element arrays, polarisation-blind DOA estimation can be implemented for conformal array antennas.

4 Array configurations on conformal carriers

The ESPRIT algorithm requires another identical copy of one array displaced in space. Given the displacement vector $|\boldsymbol{d}|$ between paired subarrays, the phase difference caused by $\boldsymbol{d}$ for narrowband far-field sources with propagation vector $\boldsymbol{u}_i$ can be expressed as $\exp(-jk_0\boldsymbol{d}\cdot\boldsymbol{u}_i)$. Since the period of $\exp(-jk_0\boldsymbol{d}\cdot\boldsymbol{u}_i)$ is 2π, the phase $-k_0\boldsymbol{d}\cdot\boldsymbol{u}_i$ is $-\pi \leq -k_0\boldsymbol{d}\cdot\boldsymbol{u}_i \leq \pi$ in order to avoid phase ambiguity. The constant $k_0 = 2\pi/\lambda$, and $-|\boldsymbol{d}| \leq \boldsymbol{d}\cdot\boldsymbol{u}_i \leq |\boldsymbol{d}|$, and so it can be derived that $|\boldsymbol{d}| \leq \lambda/2$. On this basis, the displacement vector $\boldsymbol{d}$ should be limited $|\boldsymbol{d}| \leq \lambda/2$. The signal subspaces $\boldsymbol{U}_{S1}$, $\boldsymbol{U}_{S2}$ of the paired subarrays can be obtained by eigendecomposition of the covariance matrices of their measurements. Then the rotation matrix $\boldsymbol{\psi}$ be derived, and the diagonal rotation matrix $\boldsymbol{\phi}$ of the phase difference $\exp(-jk_0\boldsymbol{d}\cdot\boldsymbol{u}_i)$ can be calculated. On this basis, the DOA can be estimated from similar matrices $\boldsymbol{\psi}$ and $\boldsymbol{\phi}$. If one parameter is estimated, one displacement vector is required by the ESPRIT algorithm. Hence, two different displacement vectors are necessary when elevation and azimuth angles all need to be found using the ESPRIT method. Therefore in order to implement blind DOA estimation for conformal arrays with respect to polarisation diversity, the following conditions are required:

1. Two pairs of subarrays with different displacement vectors should be constructed.
2. Element patterns have no effect on the displacement vectors provided in (1).
3. Parameter pairing should be implemented for the ESPRIT algorithm.

The configuration of array elements on a conformal carrier is changeful because of the varying curvature, and so the paired subarrays of ESPRIT algorithm are not easily established by actual array elements. In our work, we investigate the mechanism of the virtual array elements from FO cumulants [19], and use subarrays consisting of virtual array elements to realise high-resolution DOA estimation for conformal array antennas.

We choose virtual array elements from (15) to form new steering vectors as follows:

$$\begin{aligned}\boldsymbol{b}_1(\theta, \phi) = [&r_1 r_2 \exp\{-jk_0(\boldsymbol{p}_1 - \boldsymbol{p}_2)\boldsymbol{u}\},\\ &r_3 r_4 \exp\{-jk_0(\boldsymbol{p}_3 - \boldsymbol{p}_4)\boldsymbol{u}\}\ldots,\\ &r_{2k-1} r_{2k} \exp\{-jk_0(\boldsymbol{p}_{2k-1} - \boldsymbol{p}_{2k})\boldsymbol{u}\}]\end{aligned} \quad (19)$$

$$\begin{aligned}\boldsymbol{b}_2(\theta, \phi) = [&r_2 r_1 \exp\{-jk_0(\boldsymbol{p}_2 - \boldsymbol{p}_1)\boldsymbol{u}\},\\ &r_4 r_3 \exp\{-jk_0(\boldsymbol{p}_4 - \boldsymbol{p}_3)\boldsymbol{u}\}\ldots,\\ &r_{2k} r_{2k-1} \exp\{-jk_0(\boldsymbol{p}_{2k} - \boldsymbol{p}_{2k-1})\boldsymbol{u}\}]\end{aligned} \quad (20)$$

where

$$\boldsymbol{p}_1 - \boldsymbol{p}_2 = \boldsymbol{p}_3 - \boldsymbol{p}_4 = \cdots = \boldsymbol{p}_{2k-1} - \boldsymbol{p}_{2k} = \Delta\boldsymbol{p} \quad (21)$$

$$r_1 r_2 \neq r_3 r_4 \neq \cdots \neq r_{2k} r_{2k-1} \quad (22)$$

$$r_{2k-1}(\theta_i, \phi_i) r_{2k}(\theta_i, \phi_i) \neq r_{2k-1}(\theta_j, \phi_j) r_{2k}(\theta_j, \phi_j) \quad (23)$$

By comparing (19) with (20), we observe that the displacement vector between $\boldsymbol{b}_1(\theta, \varphi)$ and $\boldsymbol{b}_2(\theta, \varphi)$ is $2\Delta\boldsymbol{p}$ ($2\Delta\boldsymbol{p} \leq \lambda/2$) which is independent of element patterns. So the DOA can be estimated without any knowledge about element patterns for conformal array antennas utilising the ESPRIT algorithm. In order to show the generality of this method, the array configuration on conformal carriers (such as conical, cylindrical and spherical carriers) and the virtual array elements of interest are given as follows.

Conformal array antennas can be divided into several identical parts along the curved surface to tackle the 'shadow effect' of conformal carriers, so that the signals impinging on the array in a certain domain can be responded by the array elements in the same part. The global estimation results for all FOV can then be acquired by assembling all the local results. The protocol to tackle the 'shadow effect' of conformal carriers can also be used to ensure that the snapshots from every subarray consist of signals from front elements. In this paper, we divide the singly curved conformal array (such as conical, cylindrical arrays) into three parts, and each of them takes charge of the 120° azimuth domain. However, the doubly curved surface case occurs when the conformal carrier is spherical, and so the spherical conformal array should be divided twice along the doubly curved directions. The spherical conformal array is divided into six parts: three parts along the azimuth-curved surface and two parts along the elevation-curved surface. Each of the six parts takes charge of the 120° azimuth domain and 90° elevation domain. In this case, the impinging signals on the spherical array in a certain domain can be responded by all the array elements in one part. Since every part of the conformal array has the same configuration and parameter estimation mechanism, we just discuss one of them.

4.1 Array configuration on cylindrical carrier

The array structure on a cylindrical carrier is shown in Fig. 3. The global Cartesian coordinates ($\boldsymbol{X}$, $\boldsymbol{Y}$, $\boldsymbol{Z}$) are given in Fig. 3*a*. There are two array elements on every cross section and the distance vector between them is ΔP_1, $|\Delta P_1| = \lambda/4$ as shown in Fig. 3*b*. The distance vector between cross sections is ΔP_2, $|\Delta P_2| = \lambda/4$ which is explained in Fig. 3*c*. On the basis of the configuration in Fig. 3*a*, the 'extended steering vector' shown as (15) can be obtained using FO cumulants calculation of array outputs. The paired virtual array elements v_{11},v_{12} derive from paired actual array elements 1 and 2 (shown as in Fig. 3*b*), and the paired virtual array elements v_{21},v_{22} derive from paired actual array elements 1 and 3 (shown as in Fig. 3*c*), v_{11},v_{12} are counter array elements in the first paired subarrays, respectively, and v_{21},v_{22} are corresponding array elements in the second paired subarrays, respectively. According to the same mechanism, paired virtual array elements (v_{13}, v_{14}), (v_{15}, v_{16}), …, (v_{1m-1},v_{1m}),(v_{23}, v_{24}), …, (v_{2m-1}, v_{2m}) can be obtained from actual array elements. Then two pairs of subarrays can be provided and their steering vectors [shown as equations (19)–(23)] consist of virtual array elements chosen from the 'extended steering vector'. The displacement vectors of the

doi: 10.1049/iet-map.2010.0166

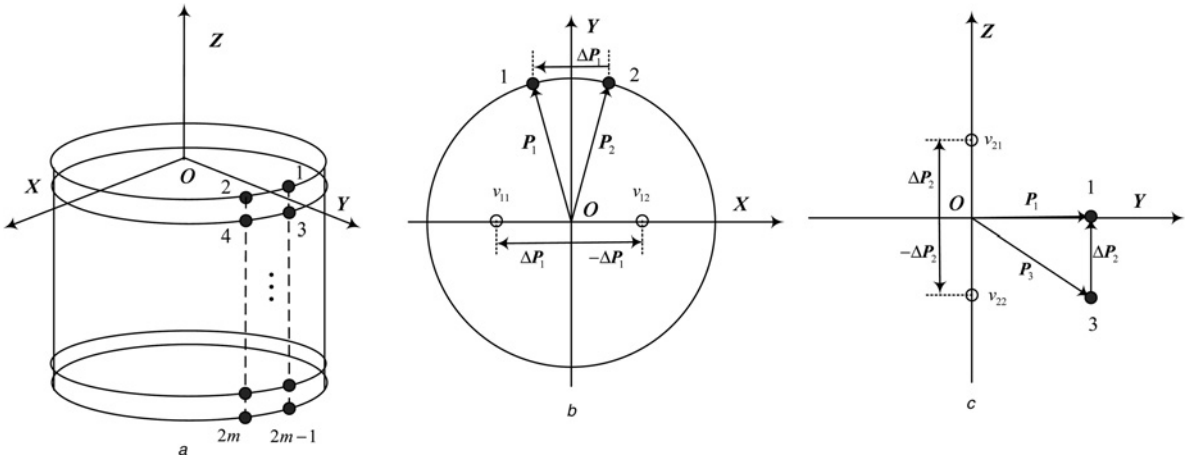

Fig. 3 *Array elements on a cylindrical carrier*

a Structure of the cylindrical conformal array
b Planform of the cylindrical conformal array
c Profile of the cylindrical conformal array

two pairs of subarrays are $\Delta \boldsymbol{P}_1$ and $\Delta \boldsymbol{P}_2$, and $\Delta \boldsymbol{P}_1 \perp \Delta \boldsymbol{P}_2$. Great convenience is given by the special relationship between $\Delta \boldsymbol{P}_1$ and $\Delta \boldsymbol{P}_2$ when the DOAs of sources are estimated.

4.2 Array configuration on a conical carrier

The array element array structure on a conical carrier is shown in Fig. 4. The global Cartesian coordinates ($\boldsymbol{X}$, $\boldsymbol{Y}$, $\boldsymbol{Z}$) are shown in Fig. 4*a*. There are three array elements on every cross section and the interval vector between paired array elements (such as paired array elements labelled by 1 and 2, 3 and 4, ..., $2m-1$ and $2m$) is $|\Delta \boldsymbol{P}_1| = \lambda/4$ illustrated in Fig. 4*b*. The distance vector between the middle paired array elements on different cross sections is $|\Delta \boldsymbol{P}_2| = \lambda/4$, and the middle array elements are mounted along the generatrix (shown as in Fig. 4*c*). On this basis, we can obtain the paired subarrays by a similar array element choosing method as used for the cylindrical array in 4.1. The displacement vectors are $\Delta \boldsymbol{P}_1$ and $\Delta \boldsymbol{P}_2$, and $\Delta \boldsymbol{P}_1 \perp \Delta \boldsymbol{P}_2$.

4.3 Array configuration on a spherical carrier

The spherical conformal array is shown in Fig. 5. The global Cartesian coordinates ($\boldsymbol{X}$, $\boldsymbol{Y}$, $\boldsymbol{Z}$) are shown in Fig. 5*a*. The array elements on a spherical carrier are divided into two parts. One part consists of array elements labelled by 1, 2, 3, 4, ..., $2m-1$, $2m$, and the other part consists of array elements labelled by $2m+1$, $2m+2$, 1, 3, 2, 4, ..., $4m-5$, $4m-4$ (which is shown in Fig. 5*a*). The interval vector between array element 1 and array element 2 is $|\Delta \boldsymbol{P}_1| = \lambda/4$ which is equal to the interval vectors between array element 3 and array element 4, array element 5 and array element 6, ..., array element $2m-1$ and array element $2m$. The interval vector between array element 1 and array element 3 is $|\Delta \boldsymbol{P}_2| = \lambda/4$ which is equal to the vectors between array element 2 and array element 4, ..., array element $4m-5$ and array element $4m-4$. On this basis, paired subarrays can be obtained according to the same mechanism mentioned above. The displacement vectors are $\Delta \boldsymbol{P}_1$ and $\Delta \boldsymbol{P}_2$, and $\Delta \boldsymbol{P}_1 \perp \Delta \boldsymbol{P}_2$.

With the above discussions, the paired subarrays can be provided utilising virtual array elements derived from actual array elements on singly curved or doubly curved surfaces by VC[3] if the actual array elements can be divided into two parts, and the paired actual array elements in the same part have the same spatial displacement $\Delta \boldsymbol{P}_1$ or $\Delta \boldsymbol{P}_2$ (shown in Figs. 3–5). The paired actual array elements can always be found on arbitrary singly curved or doubly curved

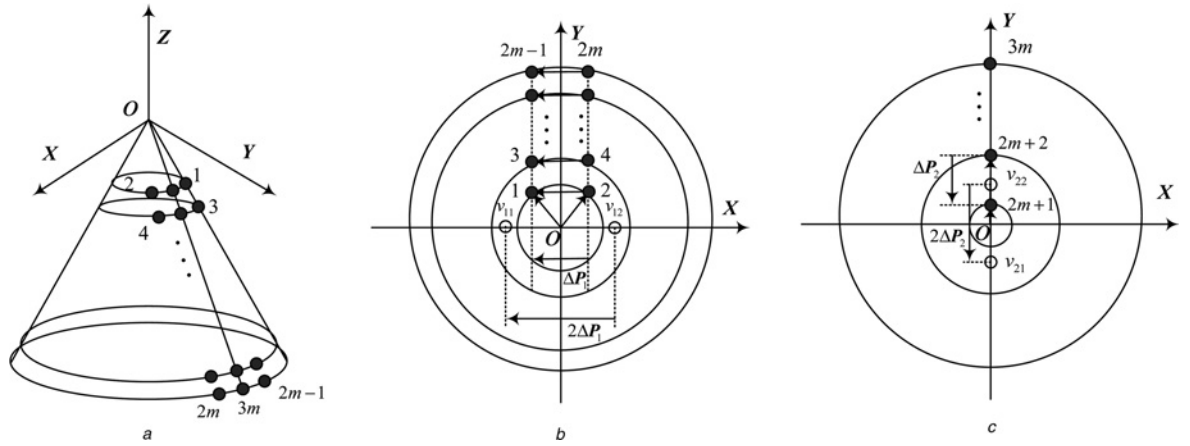

Fig. 4 *Array elements on a conical carrier*

a Structure of the conical conformal array
b Planform of the conical conformal array
c Profile of the conical conformal array

conformal surfaces by an elaborately designed array structure. On this basis, two displacement vectors $\Delta \boldsymbol{P}_1$ and $\Delta \boldsymbol{P}_2$ can be acquired from the two parts consisting of actual array elements, and the two displacement vectors $\Delta \boldsymbol{P}_1$ and $\Delta \boldsymbol{P}_2$ can also be designed having the relationship $\Delta \boldsymbol{P}_1 \perp \Delta \boldsymbol{P}_2$.

The paired subarrays required by the ESPRIT algorithm can be provided utilising array elements applicable to cylindrical, conical and spherical carriers, and the displacement vectors $\Delta \boldsymbol{P}_1$ and $\Delta \boldsymbol{P}_2$ are independent of element patterns, thus making the blind DOA estimation algorithm with respect to polarisation diversity possible. The scheme and the steps of the blind DOA estimation method are described in the following section.

5 Blind DOA estimation algorithm with respect to polarisation diversity

In this section, with a cylindrical conformal array as an example, we investigate in detail the mechanism of blind DOA estimation with respect to polarisation diversity.

The outputs of a cylindrical conformal array (shown in Fig. 3) are given as (5)–(13). The snapshots consist of a signal component emitted by independent narrowband non-Gaussian far-field sources and additive noise components which are supposed to be Gaussian random processes. In addition, the noises are independent of signals. The covariance matrix $\boldsymbol{R}_{\text{cum4}}$ of extended array measurements can be computed from (5) and (16), and the steering vectors of paired subarrays of virtual elements from 'extended steering vector' can be expressed as follows

$$\begin{aligned}\boldsymbol{b}_{11}(\theta_i, \phi_i) = &[r_1 r_2 \exp\{-\mathrm{j}k_0(\boldsymbol{p}_1 - \boldsymbol{p}_2)\cdot \boldsymbol{u}_i\},\\ &r_3 r_4 \exp\{-\mathrm{j}k_0(\boldsymbol{p}_3 - \boldsymbol{p}_4)\cdot \boldsymbol{u}_i\}\ldots,\\ &r_{2m-1} r_{2m} \exp\{-\mathrm{j}k_0(\boldsymbol{p}_{2m-1} - \boldsymbol{p}_{2m})\cdot \boldsymbol{u}_i\}]\\ = &[r_1 r_2 \exp(-\mathrm{j}k_0 \Delta \boldsymbol{p}_1 \cdot \boldsymbol{u}_i), r_3 r_4 \exp(-\mathrm{j}k_0 \Delta \boldsymbol{p}_1 \cdot \boldsymbol{u}_i)\ldots,\\ &r_{2m-1} r_{2m} \exp(-\mathrm{j}k_0 \Delta \boldsymbol{p}_1 \cdot \boldsymbol{u}_i)]\end{aligned} \tag{24}$$

$$\begin{aligned}\boldsymbol{b}_{12}(\theta_i, \phi_i) = &[r_2 r_1 \exp\{-\mathrm{j}k_0(\boldsymbol{p}_2 - \boldsymbol{p}_1)\cdot \boldsymbol{u}_i\},\\ &r_4 r_3 \exp\{-\mathrm{j}k_0(\boldsymbol{p}_4 - \boldsymbol{p}_3)\cdot \boldsymbol{u}_i\}\ldots,\\ &r_{2m} r_{2m-1} \exp\{-\mathrm{j}k_0(\boldsymbol{p}_{2m} - \boldsymbol{p}_{2m-1})\cdot \boldsymbol{u}_i\}]\\ = &[r_2 r_1 \exp(\mathrm{j}k_0 \Delta \boldsymbol{p}_1 \cdot \boldsymbol{u}_i), r_4 r_3 \exp(\mathrm{j}k_0 \Delta \boldsymbol{p}_1 \cdot \boldsymbol{u}_i)\ldots,\\ &r_{2m} r_{2m-1} \exp(\mathrm{j}k_0 \Delta \boldsymbol{p}_1 \cdot \boldsymbol{u}_i)]\end{aligned} \tag{25}$$

$$\begin{aligned}\boldsymbol{b}_{21}(\theta_i, \phi_i) = &[r_1 r_3 \exp\{-\mathrm{j}k_0(\boldsymbol{p}_1 - \boldsymbol{p}_3)\cdot \boldsymbol{u}_i\}\\ &r_3 r_5 \exp\{-\mathrm{j}k_0(\boldsymbol{p}_3 - \boldsymbol{p}_5)\cdot \boldsymbol{u}_i\},\ \ldots,\\ &r_{2m-3} r_{2m-1} \exp\{-\mathrm{j}k_0(\boldsymbol{p}_{2m-3} - \boldsymbol{p}_{2m-1})\cdot \boldsymbol{u}_i\}\\ &r_2 r_4 \exp\{-\mathrm{j}k_0(\boldsymbol{p}_2 - \boldsymbol{p}_4)\cdot \boldsymbol{u}_i\}\\ &r_4 r_6 \exp\{-\mathrm{j}k_0(\boldsymbol{p}_4 - \boldsymbol{p}_6)\cdot \boldsymbol{u}_i\},\ \ldots,\\ &r_{2m-2} r_{2m} \exp\{-\mathrm{j}k_0(\boldsymbol{p}_{2m-2} - \boldsymbol{p}_{2m})\cdot \boldsymbol{u}_i\}]\\ = &[r_1 r_3 \exp(-\mathrm{j}k_0 \Delta \boldsymbol{p}_2 \cdot \boldsymbol{u}_i),\\ &r_3 r_5 \exp(-\mathrm{j}k_0 \Delta \boldsymbol{p}_2 \cdot \boldsymbol{u}_i),\ \ldots,\\ &r_{2m-3} r_{2m-1} \exp(-\mathrm{j}k_0 \Delta \boldsymbol{p}_2 \cdot \boldsymbol{u}_i)\\ &r_2 r_4 \exp(-\mathrm{j}k_0 \Delta \boldsymbol{p}_2 \cdot \boldsymbol{u}_i),\\ &r_4 r_6 \exp(-\mathrm{j}k_0 \Delta \boldsymbol{p}_2 \cdot \boldsymbol{u}_i),\ \ldots,\\ &r_{2m-2} r_{2m} \exp(-\mathrm{j}k_0 \Delta \boldsymbol{p}_2 \cdot \boldsymbol{u}_i)]\end{aligned} \tag{26}$$

$$\begin{aligned}\boldsymbol{b}_{22}(\theta_i, \phi_i) = &[r_3 r_1 \exp\{-\mathrm{j}k_0(\boldsymbol{p}_3 - \boldsymbol{p}_1)\cdot \boldsymbol{u}_i\}\\ &r_5 r_3 \exp\{-\mathrm{j}k_0(\boldsymbol{p}_5 - \boldsymbol{p}_3)\cdot \boldsymbol{u}_i\},\ \ldots,\\ &r_{2m-1} r_{2m-3} \exp\{-\mathrm{j}k_0(\boldsymbol{p}_{2m-1} - \boldsymbol{p}_{2m-3})\cdot \boldsymbol{u}_i\},\\ &r_4 r_2 \exp\{-\mathrm{j}k_0(\boldsymbol{p}_4 - \boldsymbol{p}_2)\cdot \boldsymbol{u}_i\}\\ &r_6 r_4 \exp\{-\mathrm{j}k_0(\boldsymbol{p}_6 - \boldsymbol{p}_4)\cdot \boldsymbol{u}_i\},\ \ldots,\\ &r_{2m} r_{2m-2} \exp\{-\mathrm{j}k_0(\boldsymbol{p}_{2m} - \boldsymbol{p}_{2m-2})\cdot \boldsymbol{u}_i\}]\\ = &[r_3 r_1 \exp(\mathrm{j}k_0 \Delta \boldsymbol{p}_2 \cdot \boldsymbol{u}_i),\\ &r_5 r_3 \exp(\mathrm{j}k_0 \Delta \boldsymbol{p}_2 \cdot \boldsymbol{u}_i),\ \ldots,\\ &r_{2m-1} r_{2m-3} \exp(\mathrm{j}k_0 \Delta \boldsymbol{p}_2 \cdot \boldsymbol{u}_i)\\ &r_4 r_2 \exp(\mathrm{j}k_0 \Delta \boldsymbol{p}_2 \cdot \boldsymbol{u}_i),\\ &r_6 r_4 \exp(\mathrm{j}k_0 \Delta \boldsymbol{p}_2 \cdot \boldsymbol{u}_i),\ \ldots,\\ &r_{2m} r_{2m-2} \exp(\mathrm{j}k_0 \Delta \boldsymbol{p}_2 \cdot \boldsymbol{u}_i)]\end{aligned} \tag{27}$$

where $\Delta \boldsymbol{p}_1$, $\Delta \boldsymbol{p}_2$ are shown in Fig. 3, and $|\Delta \boldsymbol{p}_1| = |\Delta \boldsymbol{p}_2| = \lambda/4$. The element patterns satisfy the constraints in (22) and (23), then the steering vectors of paired subarrays with displacement vectors $2\Delta \boldsymbol{p}_1$ and $2\Delta \boldsymbol{p}_2$ are given by (24–27). The relationships between them take the form

$$\boldsymbol{b}_{11}(\theta_i, \phi_i) = \boldsymbol{b}_{12}(\theta_i, \phi_i) \exp(-\mathrm{j}k_0 2\Delta \boldsymbol{P}_1 \cdot \boldsymbol{u}_i) \tag{28}$$

$$\boldsymbol{b}_{21}(\theta_i, \phi_i) = \boldsymbol{b}_{22}(\theta_i, \phi_i) \exp(-\mathrm{j}k_0 2\Delta \boldsymbol{P}_2 \cdot \boldsymbol{u}_i) \tag{29}$$

Observe from (5) that, the outputs of subarray l_{11} take the form

$$\boldsymbol{X}_{11} = \boldsymbol{B}_{11}\boldsymbol{S} + \boldsymbol{N}_{11} = (\boldsymbol{B}_{11\theta}\boldsymbol{K}_{\theta} + \boldsymbol{B}_{11\phi}\boldsymbol{K}_{\phi})\boldsymbol{S} + \boldsymbol{N}_{11} \tag{30}$$

while the outputs of subarray l_{12} can be expressed as follows

$$\boldsymbol{X}_{12} = \boldsymbol{B}_{12}\boldsymbol{S} + \boldsymbol{N}_{12} = (\boldsymbol{B}_{12\theta}\boldsymbol{K}_{\theta} + \boldsymbol{B}_{12\phi}\boldsymbol{K}_{\phi})\boldsymbol{\phi}_1\boldsymbol{S} + \boldsymbol{N}_{12} \tag{31}$$

$$\boldsymbol{\phi}_1 = \mathrm{diag}[\exp(-\mathrm{j}w_{11}),\ \ldots,\ \exp(-\mathrm{j}w_{1n})] \tag{32}$$

$$\begin{aligned}w_{1i} &= (2\pi/\lambda)2\Delta \boldsymbol{P}_1 \cdot \boldsymbol{u}_i = 4\pi \Delta \boldsymbol{P}_1 \cdot \boldsymbol{u}_i/\lambda\\ &= \pi[\sin(\theta_{\Delta \boldsymbol{P}_1})\cos(\phi_{\Delta \boldsymbol{P}_1})\sin(\theta_i)\cos(\phi_i)\\ &\quad + \sin(\theta_{\Delta \boldsymbol{P}_1})\sin(\phi_{\Delta \boldsymbol{P}_1})\sin(\theta_i)\sin(\phi_i) + \cos(\theta_{\Delta \boldsymbol{P}_1})\cos(\theta_i)]\end{aligned} \tag{33}$$

where $\boldsymbol{B}_{11}$, $\boldsymbol{B}_{12}$ consist of (24) and (25) associated with signals from different bearings. Hence, the following can be obtained from subarrays l_{21}, l_{22}

$$\boldsymbol{\phi}_2 = \mathrm{diag}[\exp(-\mathrm{j}w_{21}),\ \ldots,\ \exp(-\mathrm{j}w_{2n})] \tag{34}$$

$$\begin{aligned}w_{2i} &= (2\pi/\lambda)2\Delta \boldsymbol{P}_2 \cdot \boldsymbol{u}_i = 4\pi \Delta \boldsymbol{P}_2 \cdot \boldsymbol{u}_i/\lambda\\ &= \pi[\sin(\theta_{\Delta \boldsymbol{P}_2})\cos(\phi_{\Delta \boldsymbol{P}_2})\sin(\theta_i)\cos(\phi_i)\\ &\quad + \sin(\theta_{\Delta \boldsymbol{P}_2})\sin(\phi_{\Delta \boldsymbol{P}_2})\sin(\theta_i)\sin(\phi_i) + \cos(\theta_{\Delta \boldsymbol{P}_2})\cos(\theta_i)]\end{aligned} \tag{35}$$

We can obtain the matrix $\widehat{\boldsymbol{R}}_{\text{cum4}}$ estimated from the finite array outputs for the covariance matrix $\boldsymbol{R}_{\text{cum4}}$. With eigendecomposition of $\widehat{\boldsymbol{R}}_{\text{cum4}}$, the following can be obtained

$$\widehat{\boldsymbol{R}}_{\text{cum4}} = \widehat{\boldsymbol{U}}_S \widehat{\boldsymbol{\Sigma}}_S \widehat{\boldsymbol{U}}_S^{\mathrm{H}} + \widehat{\boldsymbol{U}}_N \widehat{\boldsymbol{\Sigma}}_N \widehat{\boldsymbol{U}}_N^{\mathrm{H}} \tag{36}$$

doi: 10.1049/iet-map.2010.0166

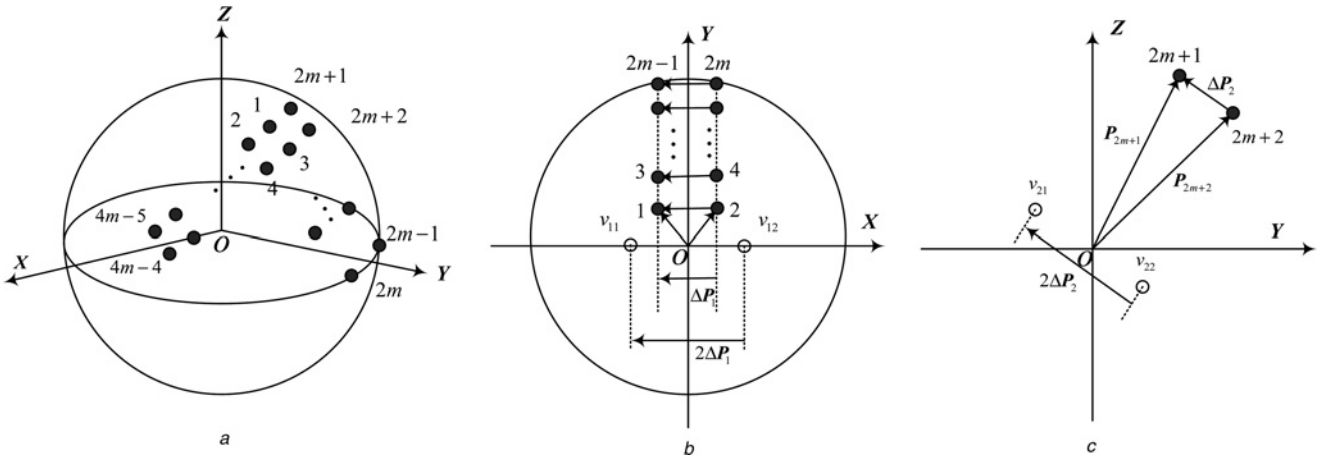

Fig. 5 *Array elements on a spherical carrier*

a Strucutre of the spherical conformal array
b Planform of the spherical conformal array
c Profile of the spherical conformal array

$\widehat{U}_S$ consists of the eigenvectors corresponding to n big eigenvalues. n is the number of sources and it is known a priori. $\widehat{U}_N$ consists of the eigenvectors corresponding to $4m^2 - n$ small eigenvalues and theoretically, $\widehat{U}_N = 0$. The range space of $\widehat{U}_S$ is the signal subspace which is also spanned by the manifold matrix $\boldsymbol{B}(\theta, \varphi)$, and therefore the

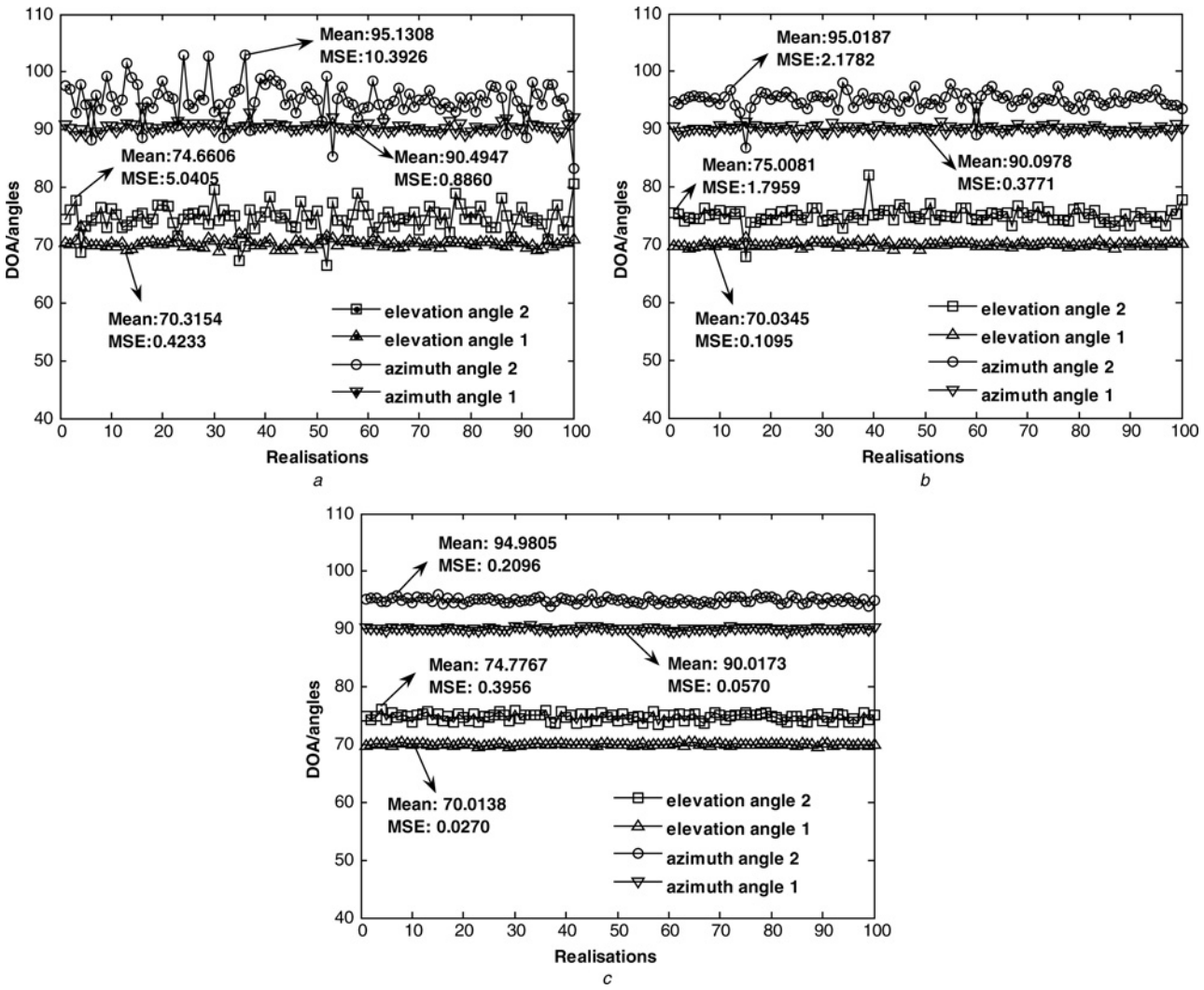

Fig. 6 *Estimation results when $L = 200$*

a SNR = 20 dB, $m = 8$
b SNR = 20 dB, $m = 16$
c SNR = 30 dB, $m = 8$

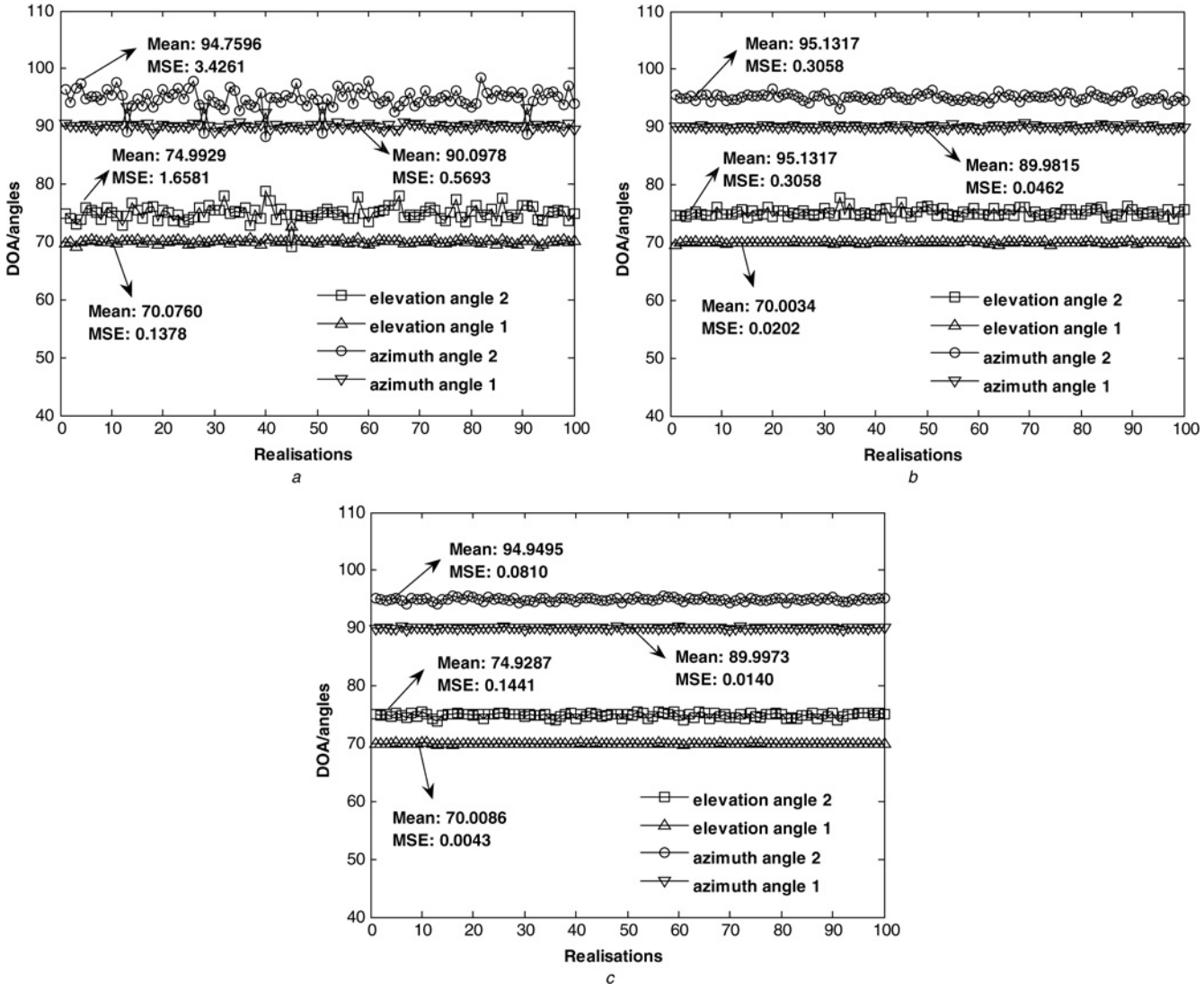

Fig. 7 *Estimation results when L = 1000*

a SNR = 20 dB, $m = 8$
b SNR = 20 dB, $m = 16$
c SNR = 30 dB, $m = 8$

relationship takes the form

$$\widehat{\boldsymbol{U}}_S = \boldsymbol{BT} \tag{37}$$

where $\boldsymbol{T}$ is a non-singular matrix. With the method of selecting array elements shown in (24)–(27), signal subspaces $\widehat{\boldsymbol{U}}_{S11}, \widehat{\boldsymbol{U}}_{S12}, \widehat{\boldsymbol{U}}_{S21}, \widehat{\boldsymbol{U}}_{S22}$ can be obtained from $\widehat{\boldsymbol{U}}_S$, and they have the following relationships

$$\text{span}\{\widehat{\boldsymbol{U}}_{S11}\} = \text{span}\{\boldsymbol{B}_{11}\} = \text{span}\{\widehat{\boldsymbol{U}}_{S12}\} = \text{span}\{\boldsymbol{B}_{12}\} \tag{38}$$

$$\text{span}\{\widehat{\boldsymbol{U}}_{S21}\} = \text{span}\{\boldsymbol{B}_{21}\} = \text{span}\{\widehat{\boldsymbol{U}}_{S22}\} = \text{span}\{\boldsymbol{B}_{22}\} \tag{39}$$

where $\boldsymbol{B}_{21}, \boldsymbol{B}_{22}$ consist of (26) and (27) associated with signals from different bearings. span{(·)} means the space spanned by the matrix (·).

Because of these relationships

$$\boldsymbol{B}_{12} = \boldsymbol{B}_{11}\boldsymbol{\phi}_1 \tag{40}$$

$$\boldsymbol{B}_{22} = \boldsymbol{B}_{21}\boldsymbol{\phi}_2 \tag{41}$$

then

$$\widehat{\boldsymbol{U}}_{S12} = \widehat{\boldsymbol{U}}_{S11}\boldsymbol{T}^{-1}\boldsymbol{\phi}_1\boldsymbol{T} = \widehat{\boldsymbol{U}}_{S11}\boldsymbol{\psi}_1 \tag{42}$$

$$\widehat{\boldsymbol{U}}_{S22} = \widehat{\boldsymbol{U}}_{S21}\boldsymbol{T}^{-1}\boldsymbol{\phi}_2\boldsymbol{T} = \widehat{\boldsymbol{U}}_{S21}\boldsymbol{\psi}_2 \tag{43}$$

Considering the least squares ESPRIT algorithm [6], we have

$$\boldsymbol{\psi}_1 = (\widehat{\boldsymbol{U}}_{S11}^{\mathrm{H}}\widehat{\boldsymbol{U}}_{S11})^{-1}\widehat{\boldsymbol{U}}_{S11}^{\mathrm{H}}\widehat{\boldsymbol{U}}_{S12} \tag{44}$$

$$\boldsymbol{\psi}_2 = (\widehat{\boldsymbol{U}}_{S21}^{\mathrm{H}}\widehat{\boldsymbol{U}}_{S21})^{-1}\widehat{\boldsymbol{U}}_{S21}^{\mathrm{H}}\widehat{\boldsymbol{U}}_{S22} \tag{45}$$

where $(\cdot)^{-1}$ denotes the inverse of matrix (·). The eigenvalues of $\boldsymbol{\psi}_1$, $\boldsymbol{\psi}_2$ are equal to the elements in diagonal matrices $\boldsymbol{\phi}_1$, $\boldsymbol{\phi}_2$. Suppose that the ith eigenvalues of $\boldsymbol{\psi}_1$, $\boldsymbol{\psi}_2$ are t_{1i}, t_{2i}, respectively, then the following can be obtained with the help of (33) and (35)

$$\exp(-\mathrm{j}w_{1i}) = t_{1i} \tag{46}$$

$$\exp(-\mathrm{j}w_{2i}) = t_{2i} \tag{47}$$

doi: 10.1049/iet-map.2010.0166

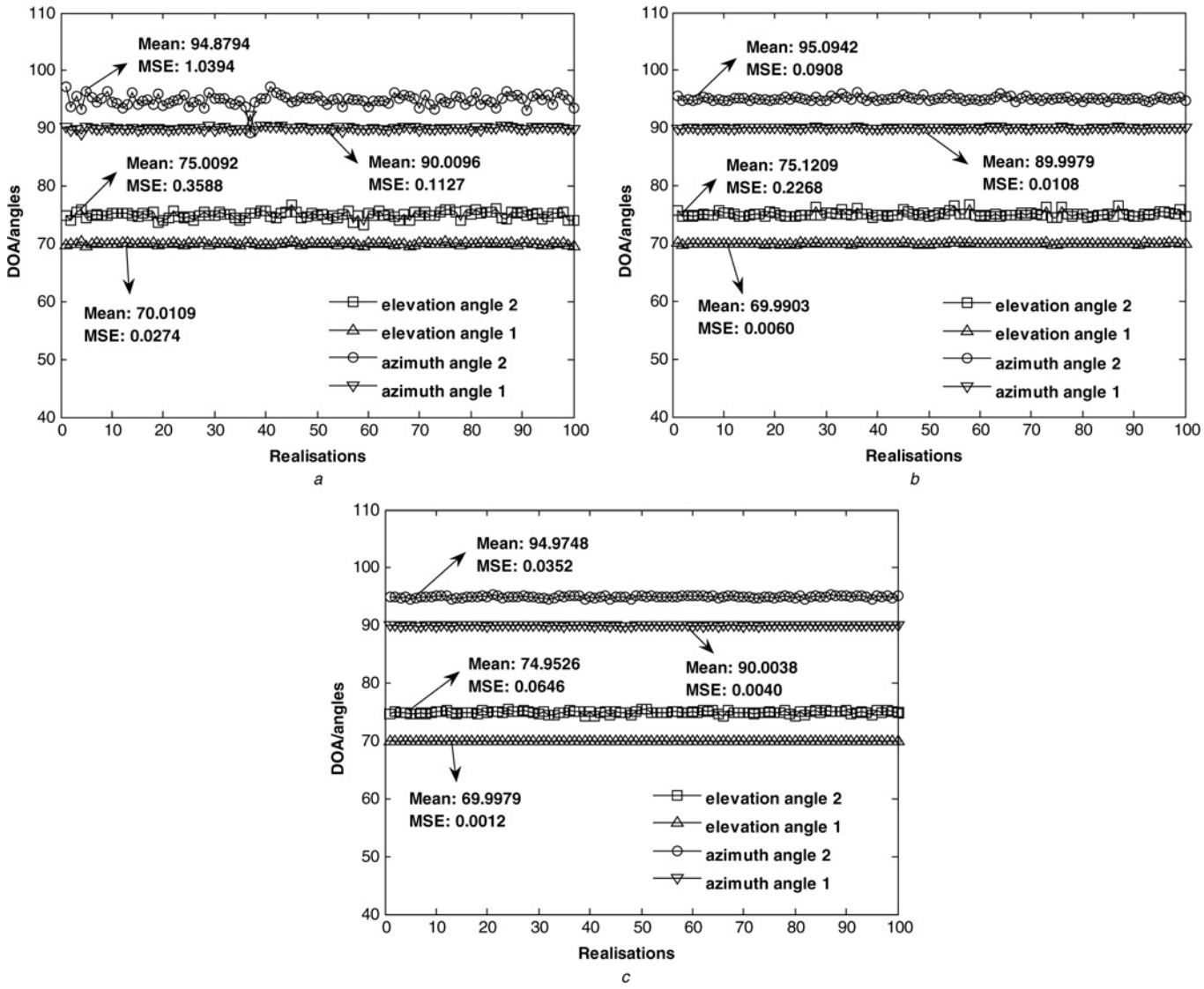

Fig. 8 *Estimation results when L = 3000*

a SNR = 20 dB, $m = 8$
b SNR = 20 dB, $m = 16$
c SNR = 30 dB, $m = 8$

Observe from Fig. 2 that, $\theta_{\Delta \boldsymbol{P}_1} = 90^\circ$, $\phi_{\Delta \boldsymbol{P}_1} = 180^\circ$, $\theta_{\Delta \boldsymbol{P}_2} = 0^\circ$, $\phi_{\Delta \boldsymbol{P}_2} = 90^\circ$.With (33), (35), (46) and (47), the following can be derived

$$\theta_i = \text{acos}[\text{angle}(t_{2i})/\pi] \tag{48}$$

$$\phi_i = \text{acos}\{\text{angle}(t_{1i})/[-\pi \sin(\theta_i)]\} \tag{49}$$

where acos(·) denotes arc cosine of (·). angle(·) is used to obtain the phase angle of the complex number. The parameters pairing problem can easily be solved because matrices $\boldsymbol{\psi i}_1$, $\boldsymbol{\psi}_2$ have the same eigenvectors shown as in (42) and (43).

Based on the above preparation, we can summarise the polarisation-blind DOA estimation algorithm for conformal arrays as follows:

Step 1: Compute the covariance matrix $\widehat{\boldsymbol{R}}_{\text{cum}\,4}$ utilising (5) and (16).
Step 2: Obtain the signal subspace matrix $\widehat{\boldsymbol{U}}_S$ through the eigendecomposition of matrix $\widehat{\boldsymbol{R}}_{\text{cum}\,4}$.
Step 3: According to (24)–(27), $\widehat{\boldsymbol{U}}_{S11}$, $\widehat{\boldsymbol{U}}_{S12}$, $\widehat{\boldsymbol{U}}_{S21}$, $\widehat{\boldsymbol{U}}_{S22}$ are constructed from $\widehat{\boldsymbol{U}}_S$.
Step 4: Matrices $\boldsymbol{\psi}_1$, $\boldsymbol{\psi}_2$ are derived from (44) and (45).
Step 5: Eigenvalues t_{1i}, t_{2i} and matrices $\boldsymbol{T}_1$, $\boldsymbol{T}_2$ are computed by the eigendecomposition of matrices $\boldsymbol{\psi}_1$, $\boldsymbol{\psi}_2$.
Step 6: The DOAs of the sources are estimated from (48) and (49).

Similarly, we can infer that the blind DOA estimation algorithm for conical and spherical carriers with respect to polarisation diversity can be derived according to the same scheme.

6 Simulations

To demonstrate the performance of the proposed DOA estimation method, 100 Monte-Carlo experiments are provided for the case of a cylindrical conformal array.

The configuration of the array is shown in Fig. 3. The number of array elements is 16 or 32, which corresponds to that $m = 8$ or $m = 16$. The number of snapshots is $L = 200$, $L = 1000$ or $L = 3000$, the source number is $n = 2$, and the bearings

of sources are $\theta_1 = 70^\circ, \phi_1 = 90^\circ, \theta_2 = 75^\circ, \phi_2 = 95^\circ$. Without loss of generality, $k_{1\theta} = 2$, $k_{1\phi} = 3$; $k_{2\theta} = 5$, $k_{2\phi} = 4$. The element patterns are $g_{i\theta} = k^{\sin(\theta_j' - \phi_j')}$, $g_{i\phi} = k^{\cos(\theta_j' - \phi_j')}$, and $k > 1$ varied with the different positions of different array elements in the global coordinate system. The signal-to-noise ratio is SNR = 20 dB or SNR = 30 dB. The sources are assumed to be independent broadcast binary phase shift-keyed waveforms, and the noise component is assumed to be additive spatial-white Gaussian random process. The estimation results are shown in Figs. 6–8. The estimation results are improved along with the increase in array elements, SNR and data length. When the number of snapshots is $L = 200$, the mean of the estimation results is satisfactory but the mean square error (MSE) of ϕ_2 is 10.3926 which is undesirable (shown in Fig. 6*a*). When the number of snapshots is $L = 1000$, the MSE and the mean of estimation results become better (shown in Fig. 7*a*). When the number of snapshots is $L = 3000$, the results are desirable (shown in Fig. 8*a*). The number of array elements also has great effect on the estimation results. With increase in the number of array elements, the estimation results become better (shown in Figs. 6*a* and *b*, 7*a* and *b*, 8*a* and *b*). SNR also has significant effect on estimation results, and when SNR = 30 dB the estimation results are better than that of SNR = 20 dB (shown in Figs. 6*a* and *c*, 7*a* and *c*, 8*a* and *c*). From the above discussions, it is confirmed that the DOAs of independent sources can be estimated efficiently by the proposed algorithm.

7 Conclusions

With the help of VC^3 and an elaborately designed array structure, paired subarrays consisting of virtual array elements are constructed for the application of ESPRIT for conformal arrays. Based on these novel paired subarrays and favourable virtues of the pattern of virtual array elements, a blind DOA estimation algorithm with respect to polarisation diversity is proposed for cylindrical, conical and spherical carriers. Simulations results with a cylindrical conformal array demonstrate that the proposed algorithm can achieve favourable DOA estimation with no exact knowledge of the source polarisation and element patterns. Compared to the existing method, the presented algorithm is applicable to different conformal carriers and the trade-off is an increase in the computational complexity since it is based on the FO cumulants of array measurements.

8 Acknowledgments

This work was supported in part by the National Science Foundation of China under Grant (Program No. 60601016) and in part by Natural Science Basic Research Plan in Shaanxi Province of China (Program No. 2010JQ8003).

9 References

1 Josefsson, L., Persson, P.: 'Conformal array antenna theory and design' (Wiley-IEEE Press, 2006)
2 Bu-hong, W., Ying, G., Yong-liang, W.: 'Frequency-invariant pattern synthesis of conformal array with low cross-polarization', *IET Microw. Antennas Propag.*, 2008, **2**, (5), pp. 442–450
3 Schmidt, R.O.: 'Multiple emitter location and signal parameter estimations', *IEEE Trans. Antennas Propag.*, 1986, **34**, (3), pp. 276–280
4 Rao, B.D., Hari, K.V.S.: 'Performance analysis of Root-MUSIC', *IEEE Trans. ASSP*, 1989, **37**, (12), pp. 1939–1949
5 Viberg, M., Ottersten, B.: 'Sensor array processing based on subspace fitting', *IEEE Trans. Signal Process.*, 1991, **39**, (5), pp. 1110–1121
6 Roy, R., Kailath, T.: 'ESPRIT—a subspace rotation approach to estimation of parameters of cissoids in noise', *IEEE Trans. ASSP*, 1986, **34**, (10), pp. 1340–1342
7 Roy, R., Kailath, T.: 'ESPRIT—Estimation of signal parameters via rotational invariance techniques', *IEEE Trans. Acoust. Speech Signal Process.*, 1989, **37**, (7), pp. 984–995
8 Stoica, P., Nehorai, A.: 'MUSIC, maximum likelihood, and Cramer–Rao bound', *IEEE Trans. ASSP*, 1989, **37**, (5), pp. 720–741
9 Stoica, P., Nehorai, A.: 'MUSIC, maximum likelihood, and Cramer-Rao bound: further results and comparisons', *IEEE Trans. ASSP*, 1990, **38**, (12), pp. 2140–2150
10 Stoica, P., Nehorai, A.: 'Performance comparison of subspace rotation and MUSIC methods for direction estimation', *IEEE Trans. Signal Process.*, 1991, **39**, (2), pp. 446–453
11 Roy, R., Paulraj, A., Kailath, T.: 'Comparative performance of ESPRIT and MUSIC for direction-of-arrival estimation'. Proc. 20th Asilomar Conf. on Circuits, Systems, Computions, Asilomar, CA, 1987, vol, vol. 12, pp. 2344–2347
12 Rao, B.D., Hari, K.V.S.: 'Performance analysis of Root-MUSIC', *IEEE Trans. ASSP*, 1989, **37**, (12), pp. 1939–1949
13 Worms, J.G.: 'Spatial superresolution with conformal array antennas'. Proc. 2000 IEEE Radar Conf., Alexandria, VA, 2000, pp. 723–728
14 Do-hong, T., Fisch, W., Russer, P.: 'Direction finding using spectral estimation with arbitrary antenna arrays'. Proc. IEEE MTT-S Int. Microwave Symp. on Digest, 2001, pp. 1387–1390
15 Hwang, S., Sarkar, T.K.: 'Direction of arrival (DOA) estimation using a transformation matrix through singular value decomposition'. Proc. IEEE/ACES Int. Conf. on Wireless Communications and Applied Computational Electromagnetic, 2005, pp. 353–356
16 Kim, K., Sarkar, T.K.: 'DOA estimation utilising directive elements on a conformal surface'. Proc. IEEE 2003 Radar Conf., 2003, pp. 91–96
17 Bu-hong, W., Ying, G.: 'Array manifold modeling for arbitrary 3D conformal array antenna'. Proc. 2008 IEEE Int. Workshop on Antenna Technology, Chiba, Japan, 2008, pp. 562–565
18 Qi, Z.-S., Guo, Y., Wang, B.-H.: 'Performance analysis of MUSIC for conformal array'. 2007 Int. Conf. on Wireless Communications, Networking and Mobile Computing, Shanghai, China, 2007, pp. 168–171
19 Qi, Z.-S., Guo, Y., Wang, B.-H.: 'DOA estimation algorithm for conical conformal array antenna'. IET 2009 Int. Conf. on RADAR, Guilin, China, 2009, pp. 1–4
20 Dogan, M.C., Mendel, J.M.: 'Applications of cumulants to array processing – part I: aperture extension and array calibration', *IEEE Trans. Signal Process.*, 1995, **43**, (5), pp. 1200–1216
21 Poral, B., Friedlander, B.: 'Direction finding algorithms based on high-order statistics', *IEEE Trans. Signal Process.*, 1991, **39**, (9), pp. 2016–2023